Supporting information for

Indirect evidence for a Ni^{III}-oxyl oxidant in the reaction of a Ni^{II} complex with peracid

*Paolo Pirovano,[a] Abigail R. Berry,[a] Marcel Swart,[b] Aidan R. McDonald[a]**

[a]School of Chemistry and CRANN/AMBER Nanoscience Institute, Trinity College Dublin, The University of Dublin, College Green, Dublin 2, Ireland

[b]ICREA, Pg. Lluís Companys 23, 08010 Barcelona, Spain and Institut de Química Computacional i Catálisi; Universitat de Girona, Facultat de Ciéncies, Campus Montilivi, 17003 Girona, Spain

email: aidan.mcdonald@tcd.ie

Physical Methods

Electronic absorption spectra were recorded on a Hewlett Packard (Agilent) 8453 diode array spectrophotometer (190-1100 nm range) in quartz cuvettes cooled using a liquid nitrogen cooled cryostat from Unisoku Scientific Instruments (Osaka, Japan). ^{1}H and ^{13}C nuclear magnetic resonance (NMR) analyses were performed on an Agilent MR400 instrument (400.13 MHz for ^{1}H NMR and 100.61 MHz for ^{13}C NMR). Gas chromatography/mass spectrometry (GC/MS) was performed using a GCT Premier Micromass time of flight mass spectrometer. Electrospray ionization (ESI) mass spectra were acquired using a Micromass time of flight spectrometer (TOF), interfaced to a Waters 2690 HPLC, or by direct injection in the mass spectrometry instrument. Attenuated total reflectance infra-red (ATR-FTIR) spectra were recorded on a Perkin-Elmer Spectrum 100 Fourier transform infrared spectrometer. Electron paramagnetic resonance spectra were recorded on a Bruker EMX spectrometer, equipped with an Oxford Instruments CE 5396, ESR9 continuous flow cryostat and an Oxford Instruments CE 5396 precision temperature controller, using liquid nitrogen cooling.

Materials

Reactions with air-sensitive materials were conducted under an inert atmosphere using standard Schlenk techniques or in a nitrogen atmosphere glove-box. All solvents and reagents were purchased from commercial sources and used as received, unless otherwise stated. Anhydrous CH_3CN and CH_2Cl_2 were obtained by distillation over CaH_2, and anhydrous acetone was obtained by distillation over B_2O_3. *m*-CPBA was purified by dissolving in CH_2Cl_2 and washing with a pH 7.4 KH_2PO_4 buffer. Purity of the *m*-CPBA product (>95%)

was confirmed by ^{1}H NMR. *N,N'*-(2,6-diisopropylphenyl)pyridine-2,6-dicarboxamide was prepared according to a reported procedure.[1]

Synthesis of [$Ni^{II}(NCCH_3)(L)$], acetonitrile-*N,N'*-bis(2,6-diisopropylphenyl)-2,6-pyridinedicarboxamido-nickel(II), 1

The reaction was conducted under an inert (N_2) atmosphere. *N,N'*-(2,6-diisopropylphenyl)pyridine-2,6-dicarboxamide (LH_2, 0.350 g, 0.72 mmol) was dissolved in anhydrous THF (6 ml). Addition of NaH (60% dispersion in mineral oil, 0.058 g, 1.4 mmol, 2 eq.) resulted in immediate gas evolution and caused the solution to turn pale yellow. When bubbling ceased, [$Ni(OTf)_2$] (0.258 g, 0.72 mmol, 1 eq., OTf = trifluoromethanesulfonate) was added, followed by 1 mL of anhydrous CH_3CN. A red solution, with a small amount of precipitate, formed; after stirring for 1 h at room temperature, the solvent was removed *in vacuo*. The resulting solids were taken up in anhydrous CH_2Cl_2 (20 ml), filtered, and evaporated to yield the product as a red-brown powder (0.268 g, 0.46 mmol, 64%). Crystals suitable for X-ray diffraction were obtained by diffusion of Et_2O into a concentrated CH_2Cl_2 solution. δ_H (400 MHz, $CDCl_3$): 8.08 (1H, t, J = 7.7 Hz, 4-py), 7.79 (2H, d, J = 7.7 Hz, 3,5-py), 7.10-7.06 (2H, m, Ar*H*), 7.05-7.00 (4H, m, Ar*H*), 3.80 (4H, hept., C*H*(CH_3)$_2$, J = 6.9 Hz), 1.40 (12H, d, CH(C*H*$_3$)$_2$, J = 6.9 Hz), 1.40 (12H, d, CH(C*H*$_3$)$_2$, J = 6.9 Hz), 1.25 (3H, s, C*H*$_3$CN). δ_C (101 MHz, $CDCl_3$): 166.9 (N*C*=O), 151.1 (pyridine *C*H), 144.3 (aniline C_q), 141.5 (pyridine *Cq*), 141.2 (aniline C_q), 125.8 (aniline *C*H), 123.6 (pyridine *C*H), 122.7 (aniline *C*H), 122.6 (CH_3*C*N), 28.9 (*C*H(CH_3)$_2$), 24.3 (CH(*C*H$_3$)$_2$), 23.6 (CH(*C*H$_3$)$_2$), 0.7 (*C*H$_3$CN). High resolution ESI-MS (m/Z): Found: 583.2583 ([M + H]$^+$, $C_{33}H_{41}N_4NiO_2$ requires 583.2578). ν_{max} (ATR-FTIR) /cm^{-1}: 2961 (CH), 2926 (CH), 2866 (CH), 2323w

(C≡N), 2296w, 1633s (C=O), 1605 (C=O), 1462, 1441, 1370, 1360, 800m, 770s, 747, 737, 680m. λ_{max} (THF)/nm 430 (ε /M^{-1} cm^{-1} 1000), 550 sh (130).

Synthesis of [$Ni^{II}(O_2CC_6H_4Cl)(L)$]Et_4N, tetraethylammonium 3-chlorobenzoato-*N*,*N*'-bis(2,6-diisopropylphenyl)-2,6-pyridinedicarboxamido-nickelate(II), 3

A crude tetraethylammonium 3-chlorobenzoate material was prepared by metathesis of $Et_4NCl.H_2O$ (0.101 g, 0.55 mmol) and sodium 3-chlorobenzoate (0.100 g, 0.55 mmol; obtained from equimolar amounts of NaOH and 3-chlorobenzoic acid), by dissolving both in CH_3OH (5 mL), removing the solvent *in vacuo*, and taking up the residue in CH_3CN (10 mL). A white solid (presumably NaCl) was filtered off, and the oily product obtained after evaporation of CH_3CN (crude $Et_4N(O_2CC_6H_4Cl)$ was added to **1** (0.314 g, 0.54 mmol), dissolved in CH_3CN (3 ml), causing the solution to immediately turn from brown-red to bright red. After 5 minutes stirring, Et_2O (20 ml) was layered on top of the solution. Over the course of 5 days, crystals of the product formed, and were recovered by decanting the solution (0.330 g, 0.40 mmol, 74%). Crystals suitable for X-ray diffraction were identified in the product. δ_H (400 MHz, $CDCl_3$): 7.85 (1H, t, *J* = 7.7 Hz, 4-py), 7.51 (2H, d, *J* = 7.7 Hz, 3,5-py), 6.90 (1H, d, J = 7.2 Hz, $C_6H_4ClCO_2$), 6.87 – 6.70 (7H, m, Ar*H*), 6.59 (1H, d, J = 7.4 Hz), 6.53 (1H, s, 2-$C_6H_4ClCO_2$), 4.28 (4H, hept., J = 6.5 Hz, $CH(CH_3)_2$), 2.83 – 2.72 (8H, m, NCH_2CH_3), 1.33 (12H, d, J = 6.5 Hz, , $CH(CH_3)_2$), 1.13 (12H, d, J = 6.5 Hz, , $CH(CH_3)_2$), 0.95 (12H, br, NCH_2CH_3). δ_C (101 MHz, $CDCl_3$): 169.6 (C_6H_4ClC=O), 166.9 (NC=O), 152.3 (2,6-py), 145.0 (*C*q Ar.), 141.9 (*C*q Ar.), 139.6 (*C*q Ar.), 138.4 (4-py), 131.8 (*C*q Ar.), 128.0 (*C*H Ar.), 127.7 (*C*H Ar.), 127.4 (*C*H Ar.), 125.9 (*C*H Ar.), 124.0 (*C*H Ar.), 121.9 (*C*H Ar.), 121.8 (3,5-py), 52.1 (NCH_2CH_3), 28.9 ($CH(CH_3)_2$), 25.3 ($CH(CH_3)_2$), 23.5 ($CH(CH_3)_2$), 7.3

(NCH_2CH_3). High resolution ESI-MS (*m*/*Z*): Found: 696.2130 ($[Ni(ArCO_2)(L)]^-$, $C_{38}H_{41}ClN_3NiO_4$ requires 696.2139). ν_{max} (ATR-FTIR) /cm^{-1}: 3058 (CH) 2956 (CH), 2865 (CH), 1605s (C=O), 1584, 1566, 1440, 1372, 1348s, 1002, 836, 757, 744s, 682m. λ_{max} (acetone)/nm 380 (ε / M^{-1} cm^{-1} 4000), 470 sh (700).

Reaction of 1 with *m*-CPBA

The reaction was monitored by electronic absorption spectroscopy. 2 ml of a 0.5 mM acetone (or CH_3CN) solution of **1** were placed in a cuvette at 25 °C. 8 μL of a 0.25 M solution of *m*-CPBA in acetone were added under stirring. New absorption features with λ_{max} = 560 nm and a shoulder at 760 nm, slowly appeared, reaching the maximum intensity after 350 s.

Reaction of 3 with magic blue

2 ml of a 0.5 mM acetone solution of **3** were cooled to -80 °C in a cuvette. 66 μL of a freshly prepared 15 mM solution of tris(4-bromophenyl)ammoniumyl hexachloroantimonate (magic blue) in CH_3CN were added under continuous stirring. Immediately, bands attributed to the oxidised product (580 nm, shoulder at 760 nm) appeared.

The reaction was repeated on a larger scale for the analysis of decay products. **3 (**24 mg, 0.03 mmol) was dissolved in 20 mL of acetone in a Schlenk flask immersed in a CH_3CN/liquid nitrogen bath (-45 °C). Magic blue (23 mg, 1 eq.) was added under stirring, causing a change in colour from red to purple; after 10 minutes the mixture was allowed to warm up to room temperature. The acetone was evaporated, the residues taken up in CH_2Cl_2 and washed with 1 M HCl. ^1H NMR, ESI-MS, GC-MS and TLC analyses showed no formation of ligand decay (oxidised) products.

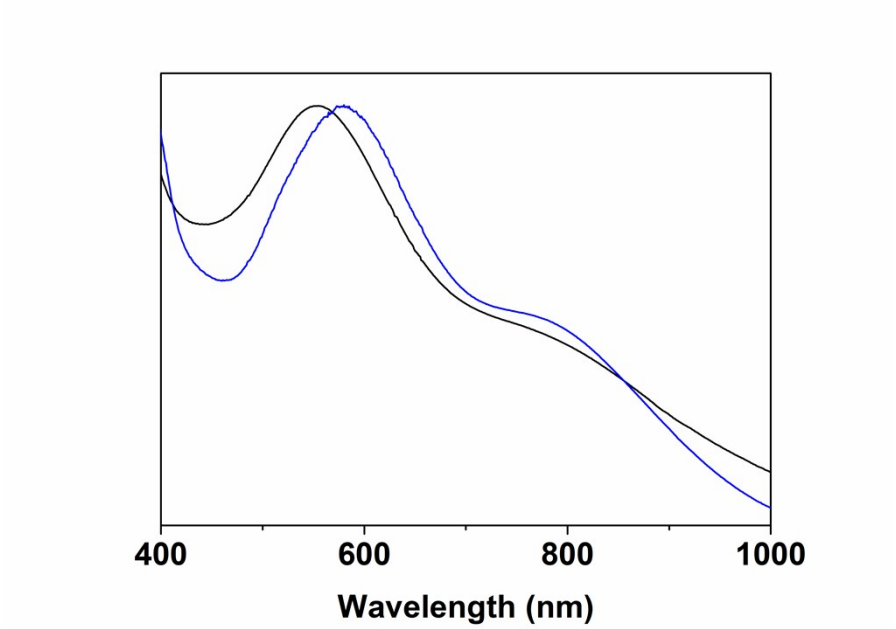

Figure S1. Normalised UV-Vis. spectra of the products obtained from the reaction of **1** and *m*-CPBA (black trace) and of **3** and magic blue (blue trace).

EPR of the Ni^{III} intermediates

The EPR spectra of the Ni^{III} intermediates were recorded on a frozen solution in an EPR tube, prepared according to the above procedure. The EPR spectrum was recorded at 77 K, 9.2 GHz, 2 W microwave power, with a 100 mT field sweep in 83 s, and 0.5 mT field modulation amplitude. Integration, simulation, and fitting were executed with Matlab and the easySpin computational package.[2] Spin quantification was effected by double integration of the signals and comparison with a standard radical sample (2,2,6,6-tetramethylpiperidin-1-yl)oxyl, TEMPO, 0.5 mM). The signals were fitted as $S = ½$ electron spin systems, with anisotropic g tensors and inhomogeneous line broadening. The spectrum of the product of the reaction of **3** + magic blue was simulated as a single species with $g_x = 2.42$, $g_y = 2.26$, $g_z = 1.99$. The

spectrum of the reaction mixture from **1** + *m*-CPBA was simulated as a mixture of the same species, plus a second species ($g_{\perp}$ = 2.23, $g_{//}$ = 2.01) in nearly equal amounts (55:45%).

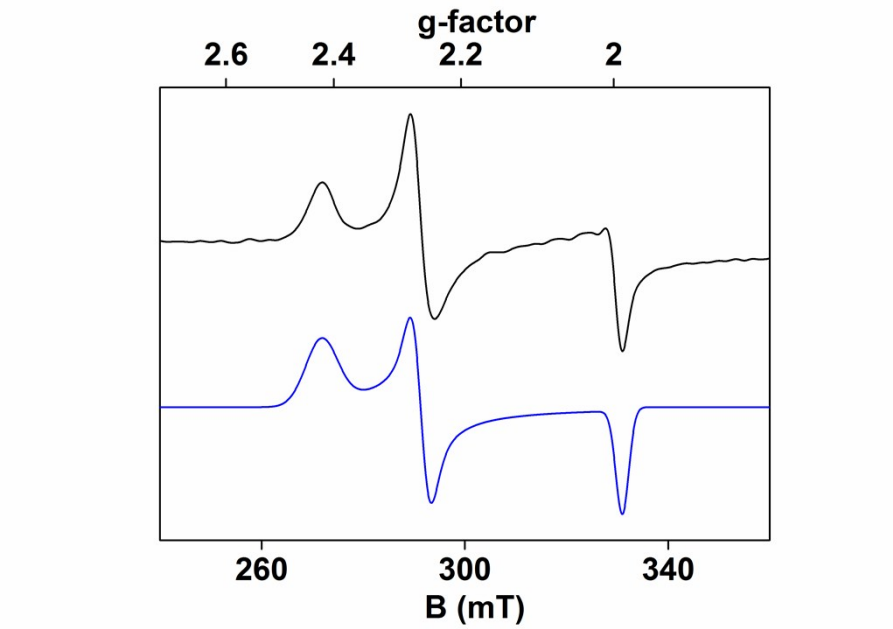

Figure S2. X-Band EPR spectrum of **2**, formed by the reaction of **3** with 1 equiv. magic blue (top) and simulated spectrum (bottom). Measured at 77 K in frozen acetone solution, 2 mW microwave power.

Mass spectrometry of the Ni^{III} species

ESI-MS analysis of the Ni^{III} species was conducted on solutions prepared according to the above procedures (**1** + *m-CPBA* and **3** + magic blue), transferred to a glass vial and diluted by 50% by the addition of cold (~ -40 °C) CH_3CN. These solutions were frozen in liquid nitrogen, and directly injected in the mass spectrometer immediately after thawing.

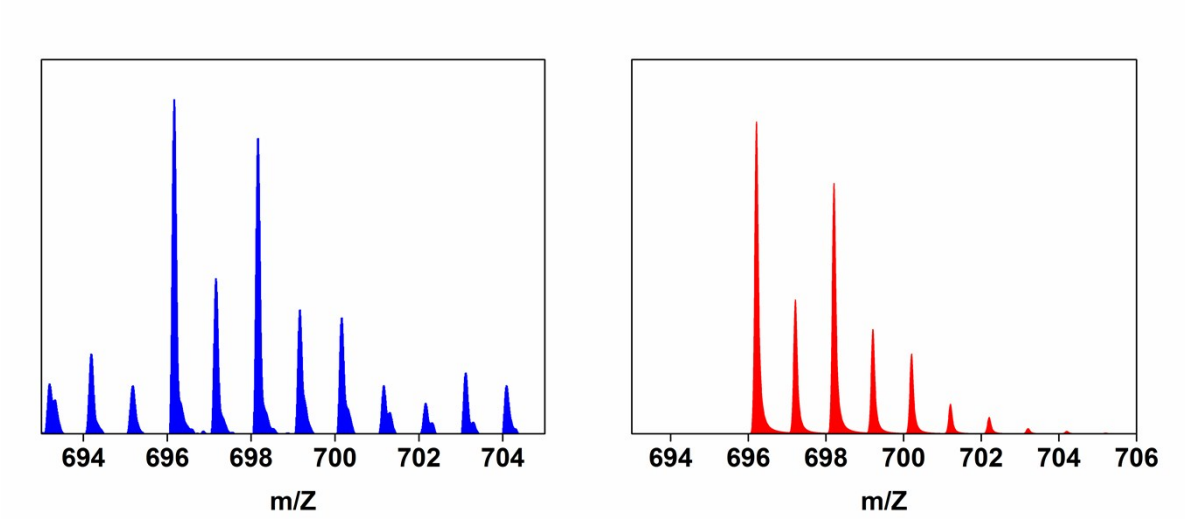

Figure S3. Positive mode ESI-MS of the mixture of **1** + *m*-CPBA (blue, left); simulation of the ion $\mathbf{2}^{+}$ ($C_{38}H_{41}ClN_3NiO_4$, m/Z = 696.2139, red, right).

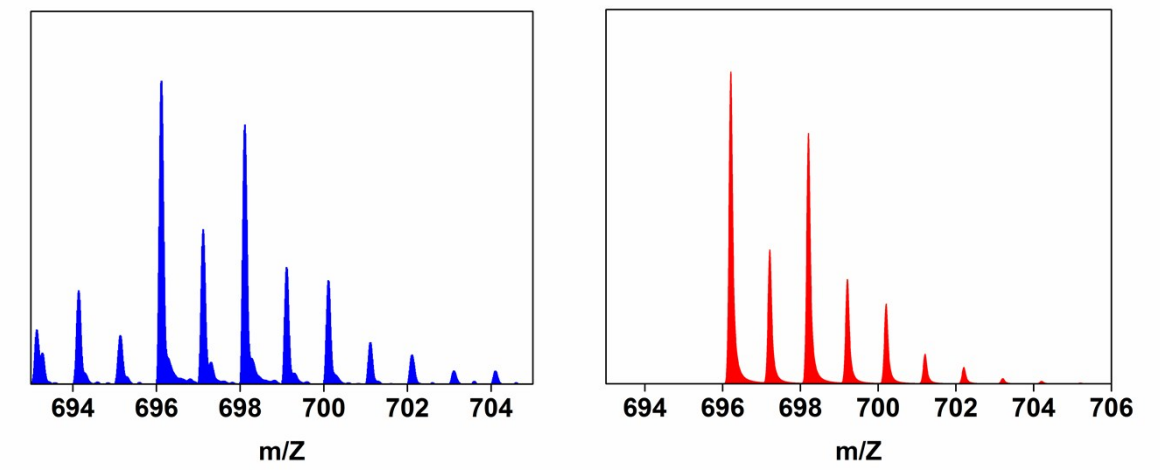

Figure S4. Positive mode ESI-MS of the mixture of **3** + magic blue (blue, left); simulation of the ion $\mathbf{2}^{+}$ ($C_{38}H_{41}ClN_3NiO_4$, m/Z = 696.2139, red, right).

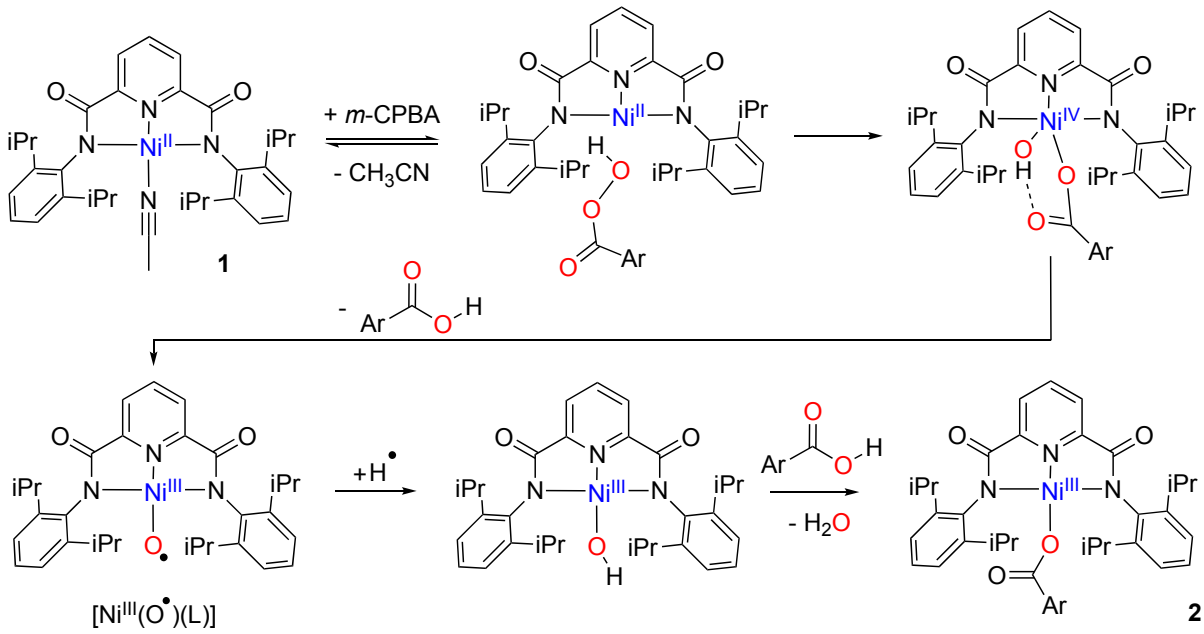

Scheme S1. Putative mechanism for the formation of **2** from the oxidation of **1** with *m*-CPBA.

Analysis of the decay products of the reaction of 1 + *m*-CPBA

The above reaction was scaled up for the structural characterization of the decay products. 227 mg of **1** (0.39 mmol) was dissolved in 100 ml of acetone in a round bottom flask and cooled in an ice-water bath. Solid *m*-CPBA (135 mg, 2 eq.) was added under stirring, causing the purple-black colour to develop over the course of a few minutes. After 1 hour, the solution was allowed to warm to room temperature and left to decay for a further 12 hours. The solvent was evaporated, the solids redissolved in CH_2Cl_2 and washed with 1 M HCl. The mixture was analysed by ESI-MS, GC-MS, and ^{1}H NMR. The compounds were isolated by column chromatographic separation on silica (eluent: hexanes/ethyl acetate 10/1). *m*-chlorobenzoic acid was not quantitatively recovered because of long elution time and strong interaction with the silica. Its amount was estimated by ^{1}H NMR integration of the crude

acidified product, using dimethylformamide as an internal standard, as >90%, based on the original *m*-CPBA amount added to the reaction mixture.

The benzoxazine **5** (Scheme S2), 2,6-diisopropylbenzoquinone (**6**) were also obtained from the separation and identified through NMR and mass spectrometry. **5** is a benzoxazine that results from the condensation of hydroxylated 2,6-diisopropylaniline and 3-chlorobenzoic acid. The quinone **6** is likely derived from the 2,6-diisopropylphenylaniline moiety of the ligand. The complementary fragment of the ligand, 6-((2,6-diisopropylphenyl)carbamoyl)picolinic acid (**7)** was observed by GC-MS (*m*/*Z* = -325.1558, $[M - H]^-$) but could not be isolated.

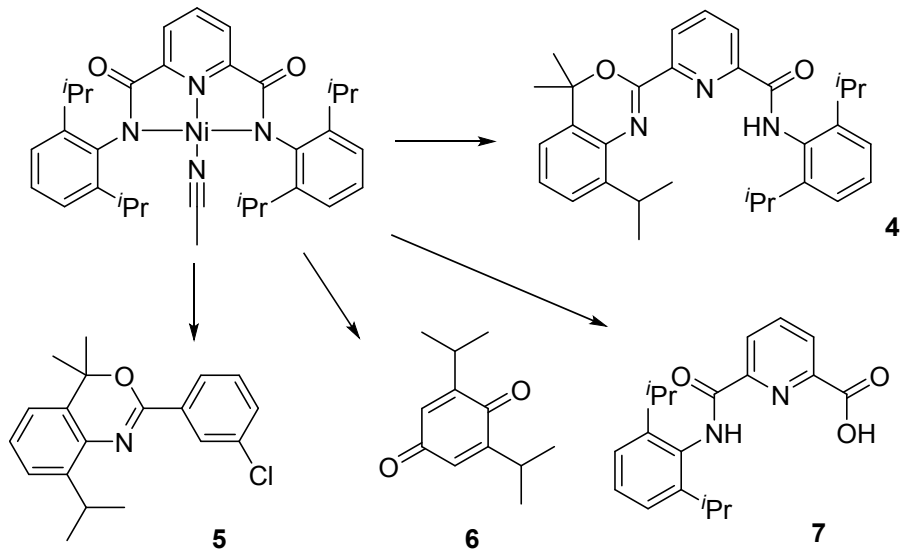

Scheme S2. Ligand degradation products identified from the post-decay mixture of **1** + *m*-CPBA.

***N*-(2,6-diisopropylphenyl)-6-(8-isopropyl-4,4-dimethyl-4H-benzo[d][1,3]oxazin-2-yl)picolinamide (4)** was isolated in 35% yield. Crystals suitable for diffraction were obtained by addition of H_2O to an ethanolic solution of **4** in an NMR tube.

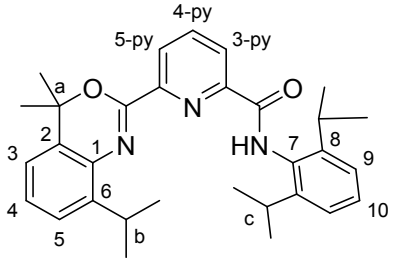

δ_H (400 MHz, $CDCl_3$): 9.74 (1H, s, N*H*), 8.49 (1H, d, *J* = 7.8 Hz, 6-py), 8.38 (1H, d, *J* = 7.8 Hz, 2-py), 8.01 (1H, t, *J* = 7.8 Hz, 4-py), 7.46 – 7.30 (1H, m, CH^{10}), 7.28 – 7.23 (3H, m, overlaps with residual $CHCl_3$, C$H^{5,9}$), 7.21 (1H, t, *J* = 7.5 Hz, CH^4), 7.01 (1H, d, J= 7.5 Hz, CH^3), 3.95 (1H, hept., *J* = 7.0 Hz, , CH^b), 3.19 (2H, hept, *J* = 6.9 Hz, CH^c), 1.72 (6H, s, CH_3^a), 1.30 (6H, d, *J* = 7.0 Hz, CH_3^b), 1.26 (12H, d, *J* = 6.9 Hz, CH_3^c). δ_C (101 MHz, $CDCl_3$): 163.1 (*C*=O), 153.7 (*C*=N), 150.2 (6-py), 149.4 (2-py), 146.1 (C^8), 144.1 (C^6), 138.0 (4-py), 135.0 (C^1), 131.4 (C^2), 131.4 (C^7), 128.1 (C^{10}), 127.3 (C^4), 126.2 (6-py), 125.3 (C^5), 123.7 (2-py), 123.6 (C^9), 119.8 (C^3), 78.9 (C^a), 29.1 (CH^c), 28.6 (CH^a), 27.4 (CH^b), 23.6 (CH_3^c), 23.39 (CH_3^b). High resolution ESI-MS (*m*/*Z*): Found: 484.2968 ([M + H]$^+$, $C_{31}H_{38}N_3O_2$ requires 484.2964).

2-(3-chlorophenyl)-8-isopropyl-4,4-dimethyl-4H-benzo[d][1,3]oxazine (5) was obtained in trace amounts (~1%).

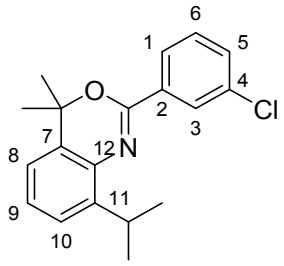

δ_H (400 MHz, $CDCl_3$): 8.12 (1H, br, CH^3), 8.07 (1H, d, J = 7.8 Hz, CH^1), 7.45 (1H, br. d, J = 7.8 Hz, CH^5), 7.38 (1H, t, J = 7.8 Hz, CH^6), 7.25 (1H, d, J = 7.6 Hz, overlaps with residual $CHCl_3$, CH^{10}), 7.17 (1H, t, J = 7.6 Hz, CH^9), 7.00 (1H, d, J = 7.6 Hz, CH^8), 3.94 (1H, hept., *J* = 7.0 Hz, CH(CH$_3$)$_2$), 1.69 (6H, s, OC(CH_3)$_2$), 1.30 (6H, d, J = 7.0 Hz, CH(CH_3)$_2$). δ_C (101 MHz, $CDCl_3$): 154.0 (*C*=N), 143.8 (C^{11}), 135.5 ($C^{2/4}$), 135.2 (C^{12}), 134.2 ($C^{4/2}$), 131.2 (C^7), 130.9 (C^1), 129.4 (C^6), 127.8 (C^3), 126.6 (C^9), 126.0 (C^5), 125.13 (C^{10}), 119.6 (C^8), 78.5 (O*C*(CH_3)$_2$), 28.3 (OC(*C*H$_3$)$_2$), 27.2 (*C*H(*C*H$_3$)$_2$), 23.4 (CH(*C*H$_3$)$_2$). ESI-MS (*m*/*Z*): Found: 314.1304 ($[M + H]^+$, $C_{19}H_{21}ClNO$ requires 314.1306).

2,6-Diisopropylbenzoquinone (**6**) was isolated in 6% yield. Spectra correspond to previous literature reports.[3] δ_H (400 MHz, $CDCl_3$): 6.47 (1H, s), 3.07 (2H, hept., J = 6.9 Hz), 1.13 (12H, d, J = 6.9 Hz).

Reaction of 1 with *m*-CPBA – isotopic labelling with $H_2{}^{18}O$

The reactions were conducted in Schlenk flasks under inert atmosphere; a blank reaction was conducted in parallel using the same nickel complex and *m*-CPBA stock solutions, and natural (non-enriched) H_2O. To a stirred solution of **1** in anhydrous CH_3CN (3 mL, 1.7 mM), 40 μL of $H_2{}^{18}O$ (97 atom% enrichment) were added, followed by 2 equivalents of *m*-CPBA. The oxidised intermediate was allowed to form and decay, and after 12 hours the solvent was removed, followed by addition of CH_2Cl_2 and washing with 1 M HCl. The isotopic content of the products was analysed by ESI-MS. A complicating factor was that [^{18}O]**4** has the same nominal mass as unmodified LH_2. Nevertheless, the corresponding peak was 50% more intense in the experiment with $H_2{}^{18}O$, as opposed to a blank with natural abundance water, after normalising the peak corresponding to **4** (Figure S5). The extent of ^{18}O incorporation in the product was evaluated as ~30%, after subtracting the peak intensity due to LH_2.

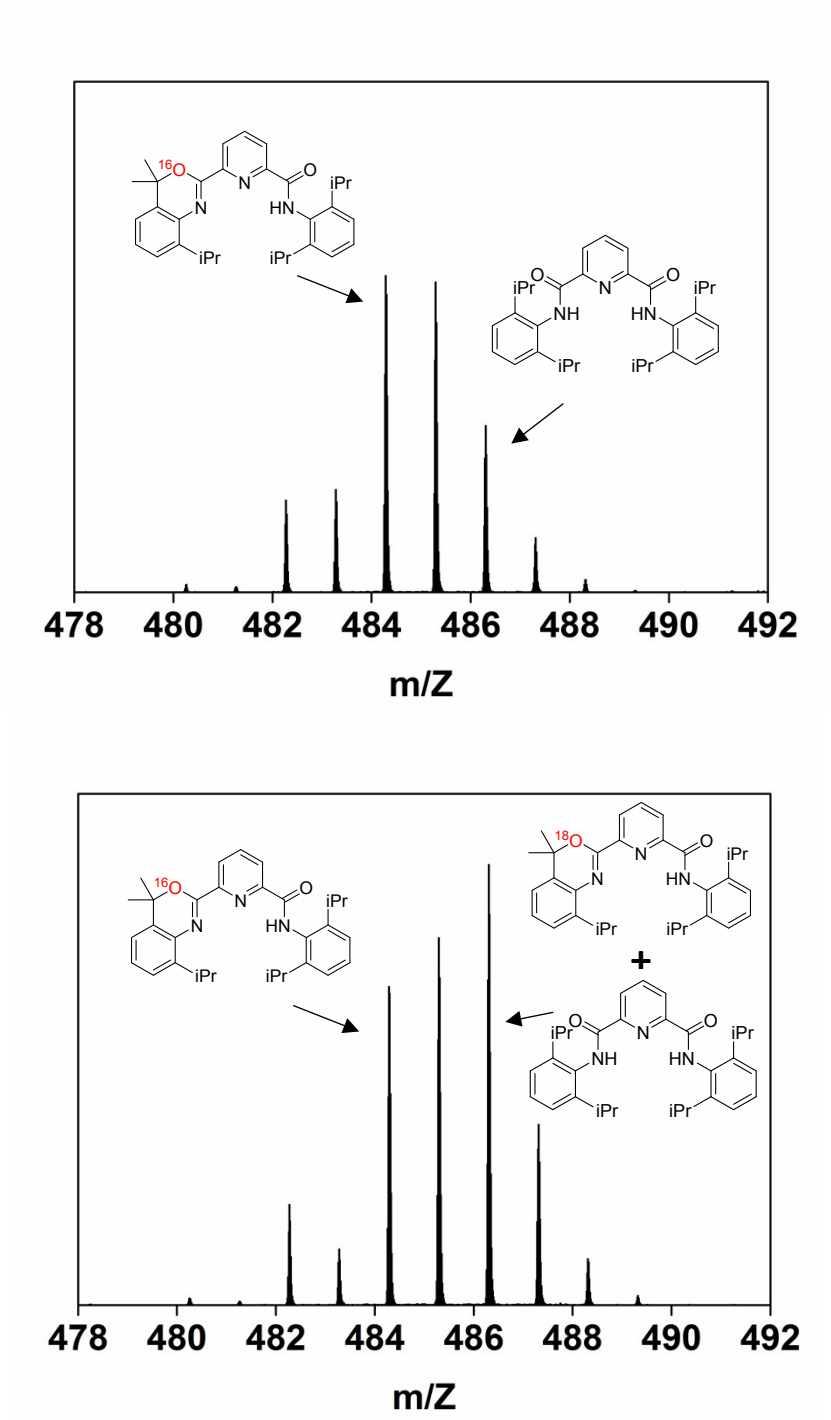

Figure S5. ESI-MS of the post-decay mixtures of (**1** + *m*-CPBA*)* in the presence of excess H_2O (natural abundance, top) and $H_2{}^{18}O$ (bottom).

Reaction of *N*,*N'*-(2,6-diisopropylphenyl)pyridine-2,6-dicarboxamide with *m*-CPBA

N,*N'*-(2,6-diisopropylphenyl)pyridine-2,6-dicarboxamide (200 mg, 0.41 mmol) was dissolved in 40 mL of acetone and solid *m*-CPBA (156 mg, 0.91 mmol, 2.2 eq.) added to it under stirring. After 24 h an NaI test indicated the presence of unreacted oxidant; this was carefully quenched with aqueous $Na_2S_2O_3$. The crude mixture was analysed by ^{1}H NMR, ESI-MS, GC-MS and TLC, where no products other than the unmodified ligand LH_2 were identified.

Reaction of 1 with *m*-CPBA – effect of [D_6]acetone medium

1 (0.010 g, 0.021 mmol) was dissolved in 2 mL of [D_6]-acetone. *m*-CPBA (0.07 g, 0.041 mmol, 2 eq.) was subsequently added, causing the solution to turn dark purple. A parallel experiment was conducted according to the identical procedure, but using [H_6]-acetone instead of [D_6]-acetone. The two solutions were then allowed to decay. The purple coloration of the protic acetone solution completely disappeared in < 8 h, leaving a yellow solution; conversely, the same happened for the [D_6]acetone solution in ~26 h.

After a total of 30 h, 2-bromoacetophenone (5.5 mg) was added to each of the mixtures, to function as an internal NMR standard. The solutions were acidified with 1 M HCl, then the solvent was evaporated, and the residue re-dissolved in $CDCl_3$, dried over $MgSO_4$, filtered through a cotton plug and analysed by ^{1}H NMR . The relative integration of the peaks of **4** (3.95 ppm, 1H), and of 2-bromoacetophenone (4.46 ppm, 2H), showed equal formation of **4** in the two reactions, within the accuracy of the NMR quantification (~35% based on the initial amount **1**).

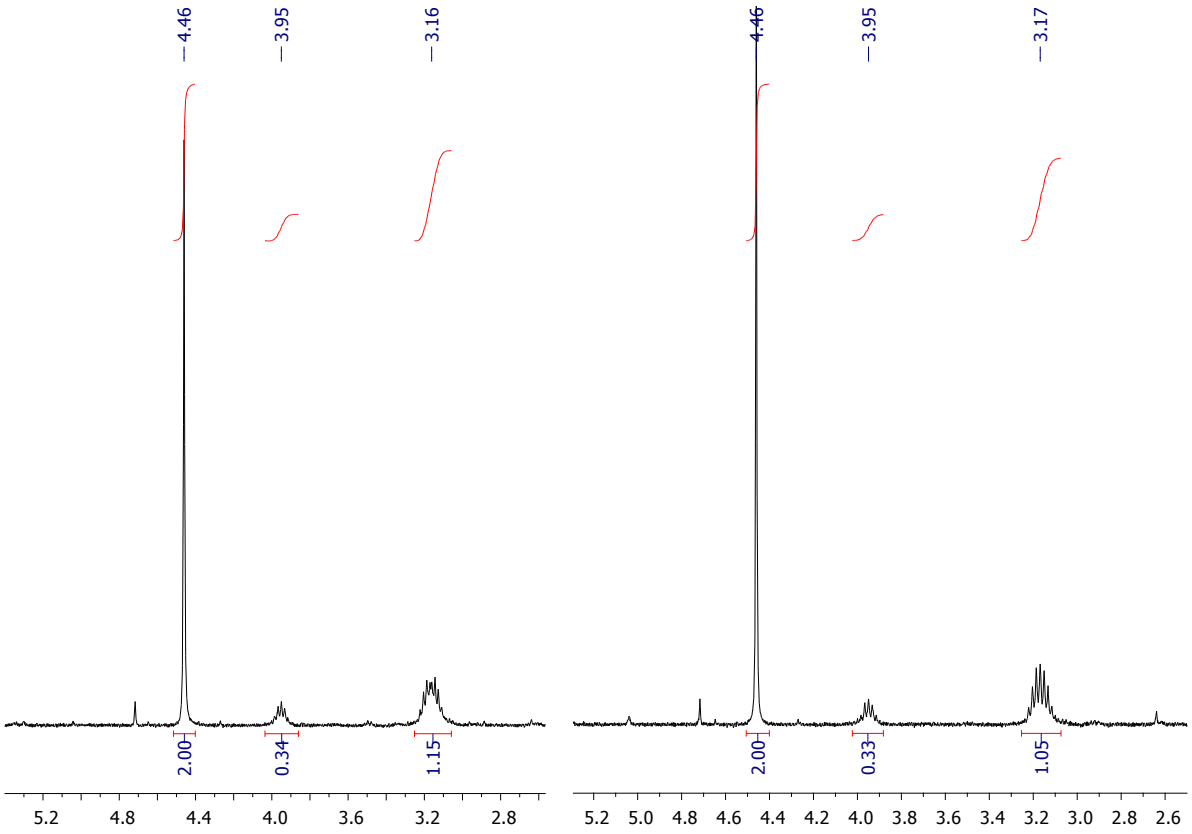

Figure S6. Expansions of the ^{1}H NMR spectra of the post-reaction mixtures of the reactions of **1** + *m*-CPBA in [D_6]acetone (left) and acetone of natural isotopic composition (right). The peaks corresponding to the internal standard (PhCOC*H*$_2$Br, 4.46 ppm) and of the isopropyl groups of **4** (3.95 ppm) and LH_2 (3.19 ppm).

Oxidation of cyclohexane

1 (5 mg, 8.6 μmol) was dissolved in 1 mL of [*D*$_6$]acetone; 4 mL of cyclohexane was added to the solution, followed by *m*-CPBA (3 mg, 17 μmol, 2 eq.). The mixture was allowed to react and decay under stirring for 12 hours; afterwards it was filtered on a cotton plug and analysed by GC-MS. A blank experiment was conducted under the same conditions, but without the presence of nickel complex.

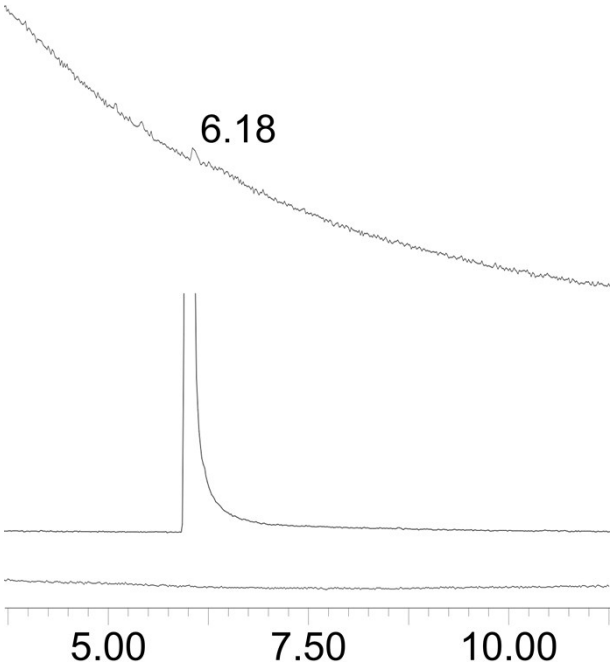

Figure S7. GC-MS chromatograms of the post reaction mixture of **1** + *m*-CPBA in the presence of cyclohexane (top), an authentic pure sample of cyclohexanol (middle), and of cyclohexane + *m*-CPBA (bottom).

X-Ray diffraction methods

Single crystal X-ray data were collected at 100(2) K on a Bruker Apex II CCD diffractometer using graphite-monochromated Mo-Kα radiation (λ = 0.71073 Å), an Oxford Cryosystems Cobra low temperature device and a MiTeGen micromount. Bruker APEX software[4] was used to correct for Lorentz and polarisation effects. The structures were solved and refined using the Bruker SHELXTL Software Package.[5]

Table S1. Crystal data and structure refinement parameters for **1**, **3**, and **4**.

	1	**3**	**4**
Empirical formula	$C_{70}H_{90}N_8Ni_2O_5$	$C_{31}H_{64}ClN_5NiO_4$	$C_{33}H_{43}N_3O_3$
Formula weight	1240.92	869.40	529.70
Temperature	100(2) K	100(2) K	100(2) K
Wavelength	0.71073 Å	0.71073 Å	1.54178 Å
Crystal system	Monoclinic	Triclinic	Hexagonal
Space group	P 1 2_1/c 1	Pī	$P6_5$
Unit cell dimensions	a = 20.7514(7) Å α= 90° b = 21.5643(8) Å β= 110.8990(10)° c = 16.1479(6) Å γ = 90°	a = 11.2143(4) Å α= 110.6620(10)° b = 13.9431(5) Å β= 91.4110(10) ° c = 16.1500(6) Å γ = 106.7540(10)°	a = 8.7435(4) Å α= 90° b = 8.7435(4) Å β= 90° c = 69.045(3) Å γ = 120°
Volume	3258.95(19) $Å^3$	2239.91(14) $Å^3$	2276.8(3) $Å^3$
Z	4	2	6
Density (calculated)	$1.221 \cdot 10^3$ kg/m^3	$1.289 \cdot 10^3$ kg/m^3	$1.155 \cdot 10^3$ kg/m^3
Absorption coefficient	0.612 mm^{-1}	0.542 mm^{-1}	0.581 mm^{-1}
F(000)	2648	928	1716
Crystal size	0.050 x 0.150 x 0.180 mm^3	0.260 x 0.230 x 0.110 mm^3	0.21 x 0.19 x 0.04 mm^3
Theta range for data collection	1.41 to 27.51°	2.298 to 30.633°	3.841 to 68.386°
Index ranges	$-26 \le h \le 26$, $-28 \le k \le 28$, $-20 \le l \le 20$	$-16 \le h \le 16$, $-19 \le k \le 19$, $-23 \le l \le 23$	$-10 \le h \le 10$, $-10 \le k \le 10$, $-82 \le l \le 82$
Reflections collected	72448	49339	26441
Independent reflections	15480 [R(int) = 0.0443]	13768 [R(int) = 0.0318]	5575 [R(int) = 0.0588]
Absorption correction	Semi-empirical from equivalents	Semi-empirical from equivalents	Semi-empirical from equivalents
Max. and min. transmission	0.9701 and 0.8979	0.7461 and 0.6825	0.7531 and 0.5659
Refinement method	Full-matrix least-squares on F^2	Full-matrix least-squares on F^2	Full-matrix least-squares on F^2
Data / restraints / parameters	15480 / 16 / 795	13768 / 0 / 545	5575 / 8 / 384
Goodness-of-fit on F2	1.020	1.025	1.031
Final R indices [I>2σ(I)]	R1 = 0.0402, wR2 = 0.0917	R1 = 0.0370, wR2 = 0.0881	R1 = 0.0577, wR2 = 0.1461
R indices (all data)	R1 = 0.0658, wR2 = 0.1019	R1 = 0.0505, wR2 = 0.0954	R1 = 0.0653, wR2 = 0.1516
Largest diff. peak and hole	0.750 and -0.720 e.$Å^{-3}$	0.551 and -0.518 e.$Å^{-3}$	0.256 and -0.227 e.$Å^{-3}$

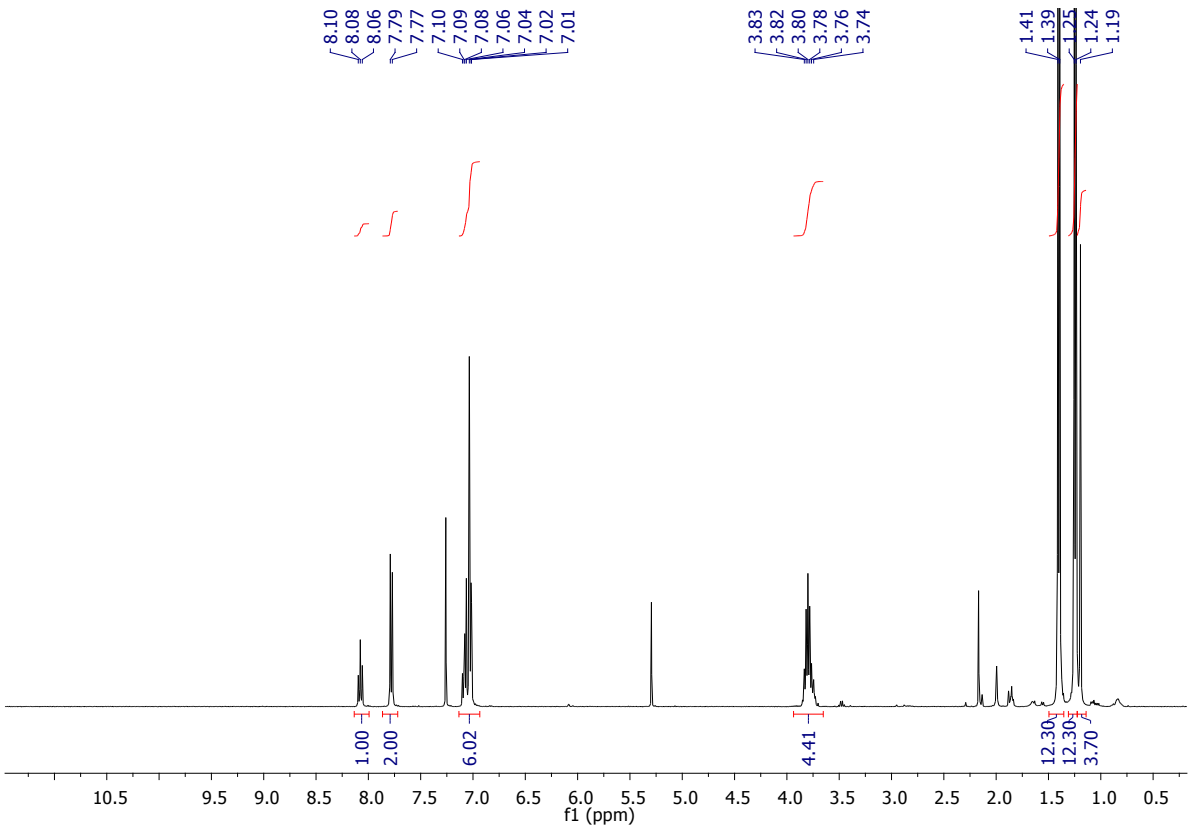

Figure S8. ^{1}H NMR spectrum of **1** (400 MHz, $CDCl_3$).

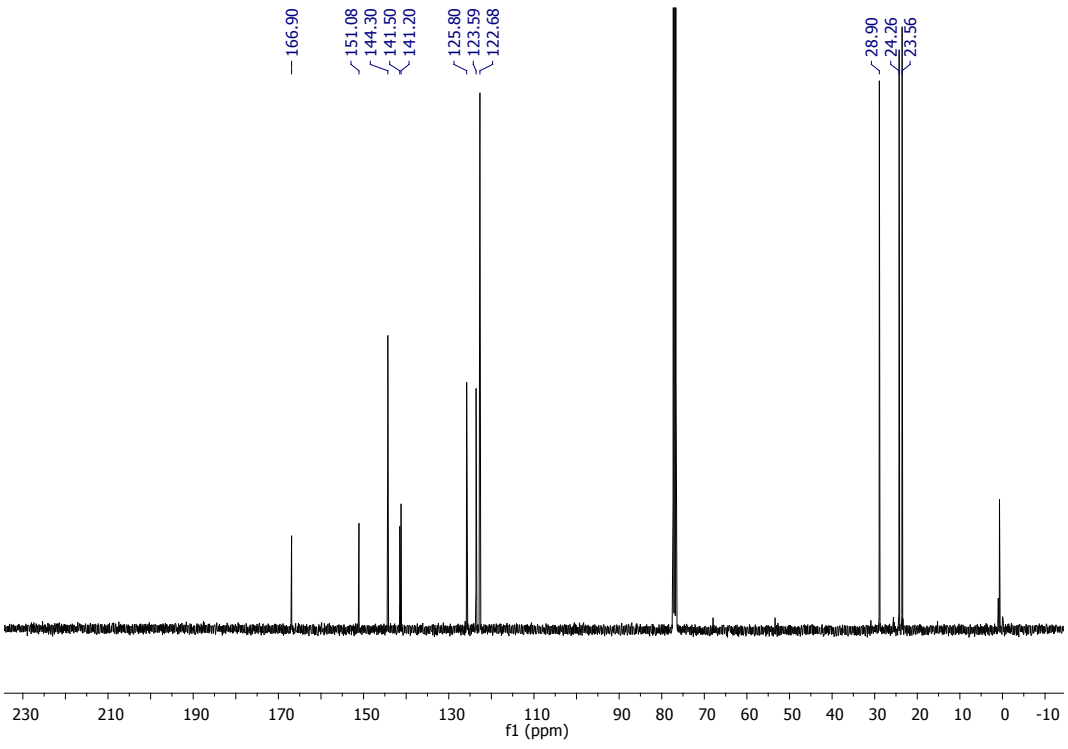

Figure S9. ^{13}C NMR spectrum of **1** (101 MHz, $CDCl_3$).

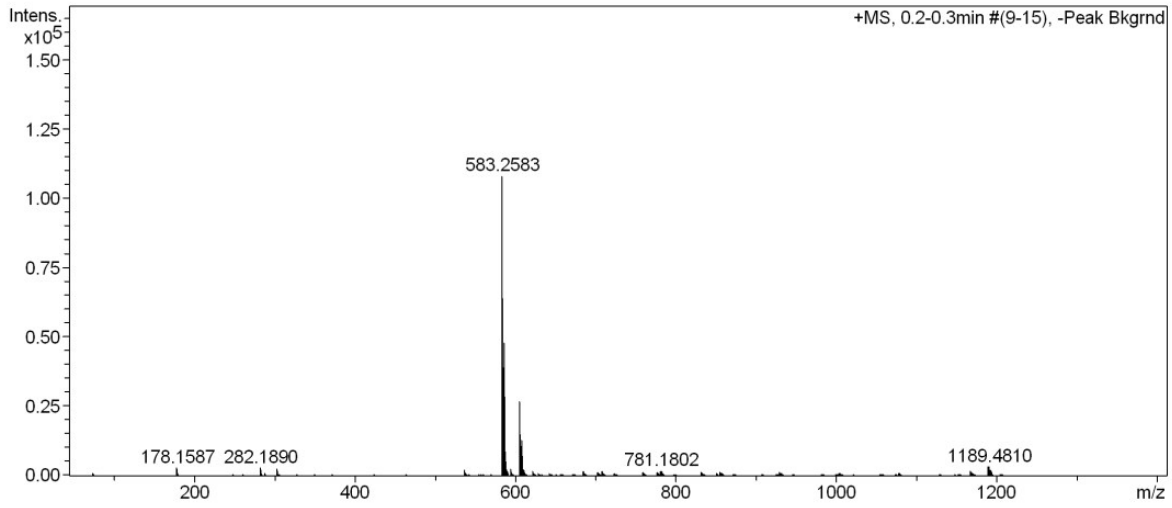

Figure S10. Positive mode ESI MS spectrum of **1**; [**1** + H]$^+$, $C_{33}H_{41}N_4NiO_2$ requires 583.2578.

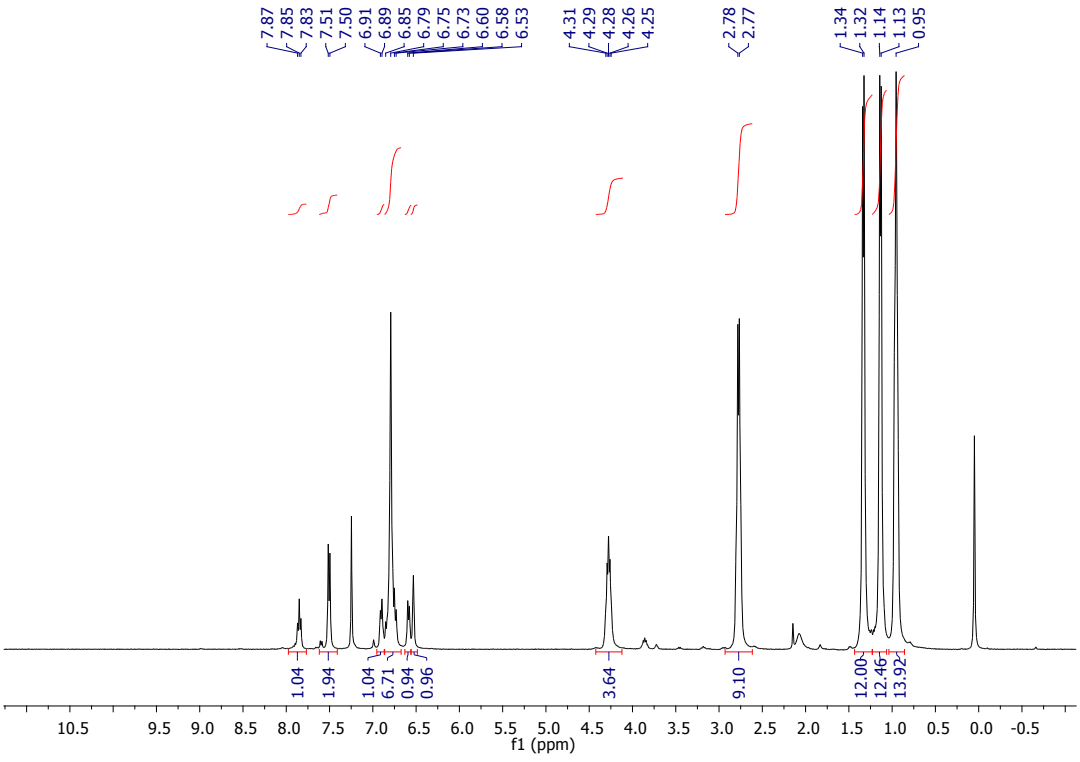

Figure S11. ^{1}H NMR spectrum of **3** (400 MHz, $CDCl_3$).

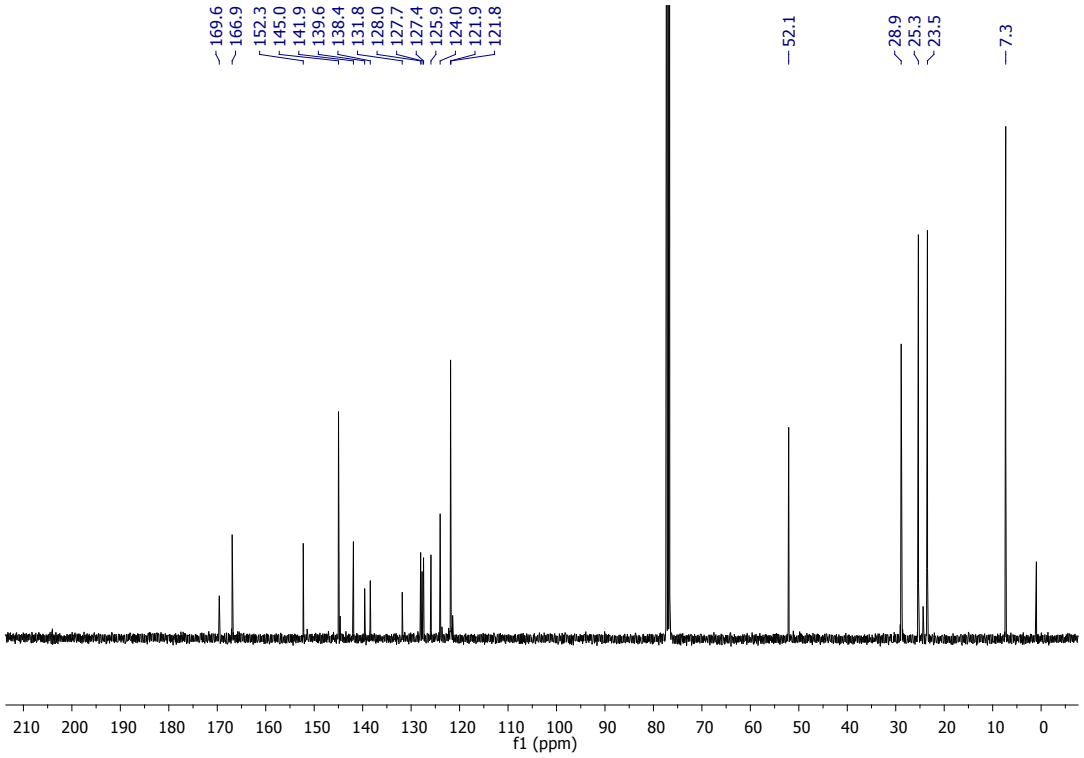

Figure S12. ^{13}C NMR spectrum of **3** (101 MHz, $CDCl_3$).

*

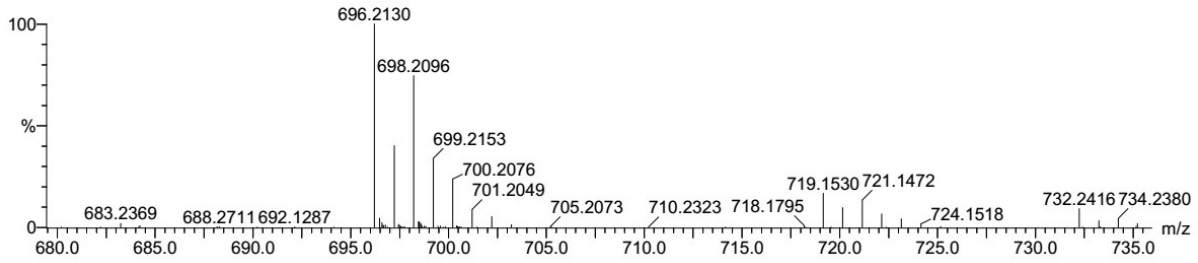

Figure S13. Negative mode ESI MS spectrum of **3**; $[Ni(ArCO_2)(L)]^-$, $C_{38}H_{41}ClN_3NiO_4$ requires 696.2139.

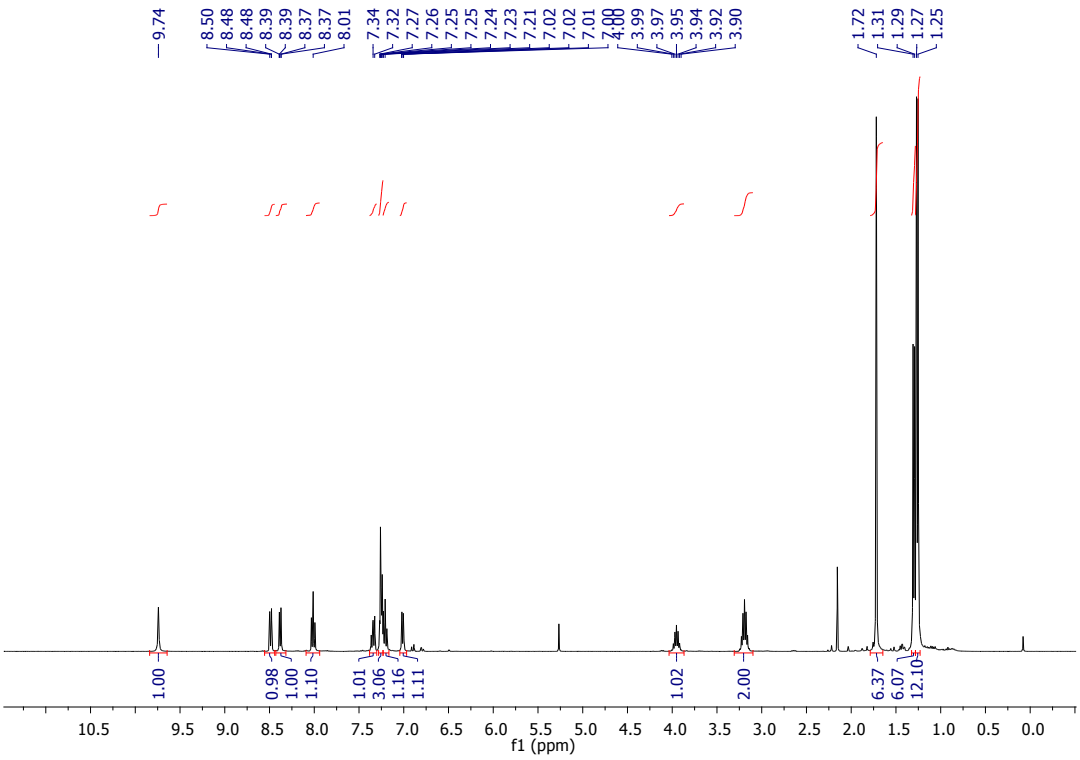

Figure S14. ^{1}H NMR spectrum of **4** (400 MHz, $CDCl_3$).

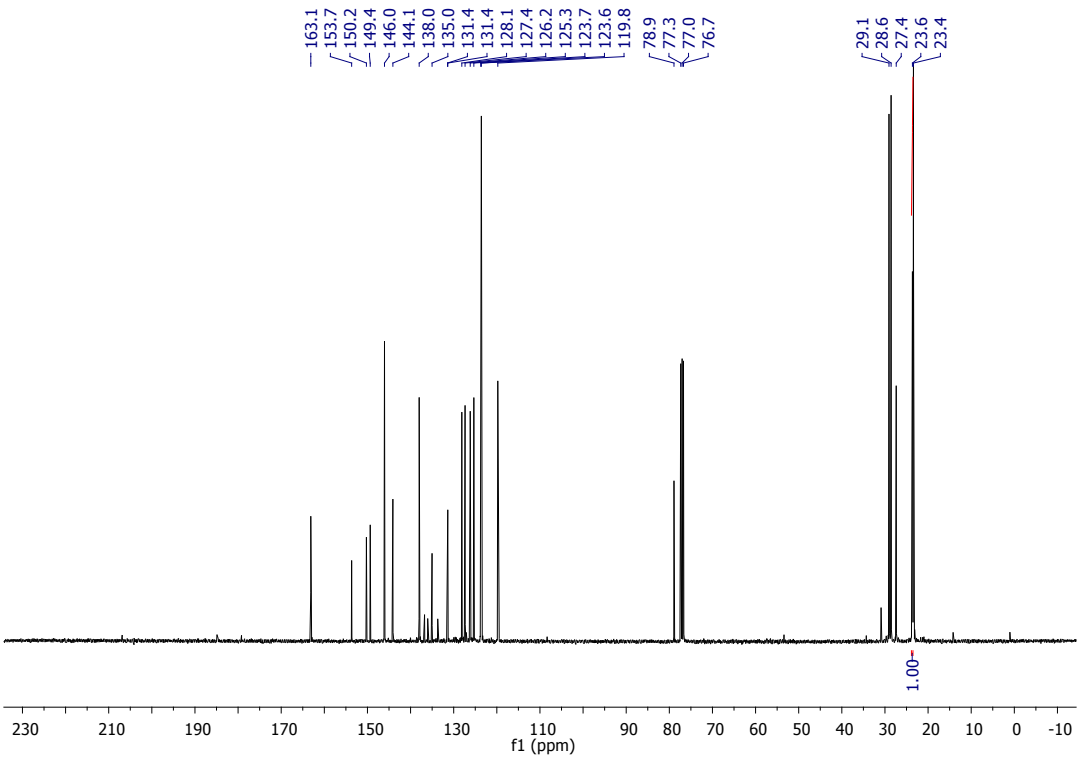

Figure S15. ^{13}C NMR spectrum of **4** (101 MHz, $CDCl_3$).

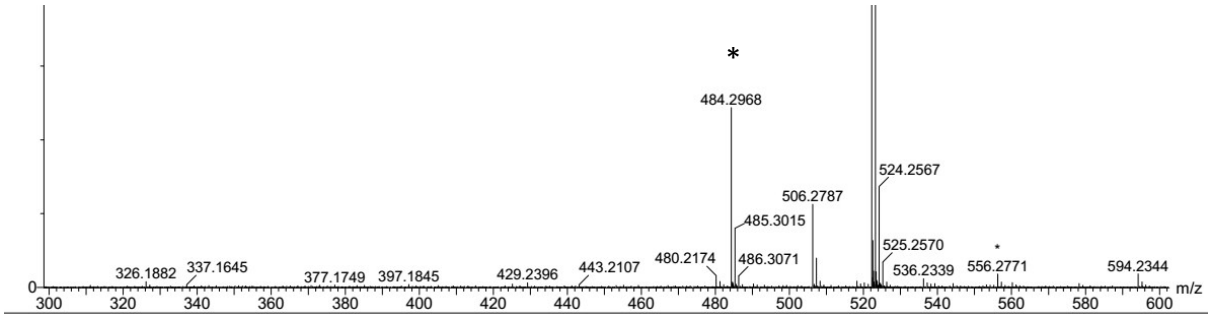

Figure S16. Positive mode ESI MS spectrum of **4**; $[\mathbf{4} + H]^+$, $C_{31}H_{38}N_3O_2$ requires 484.2964.

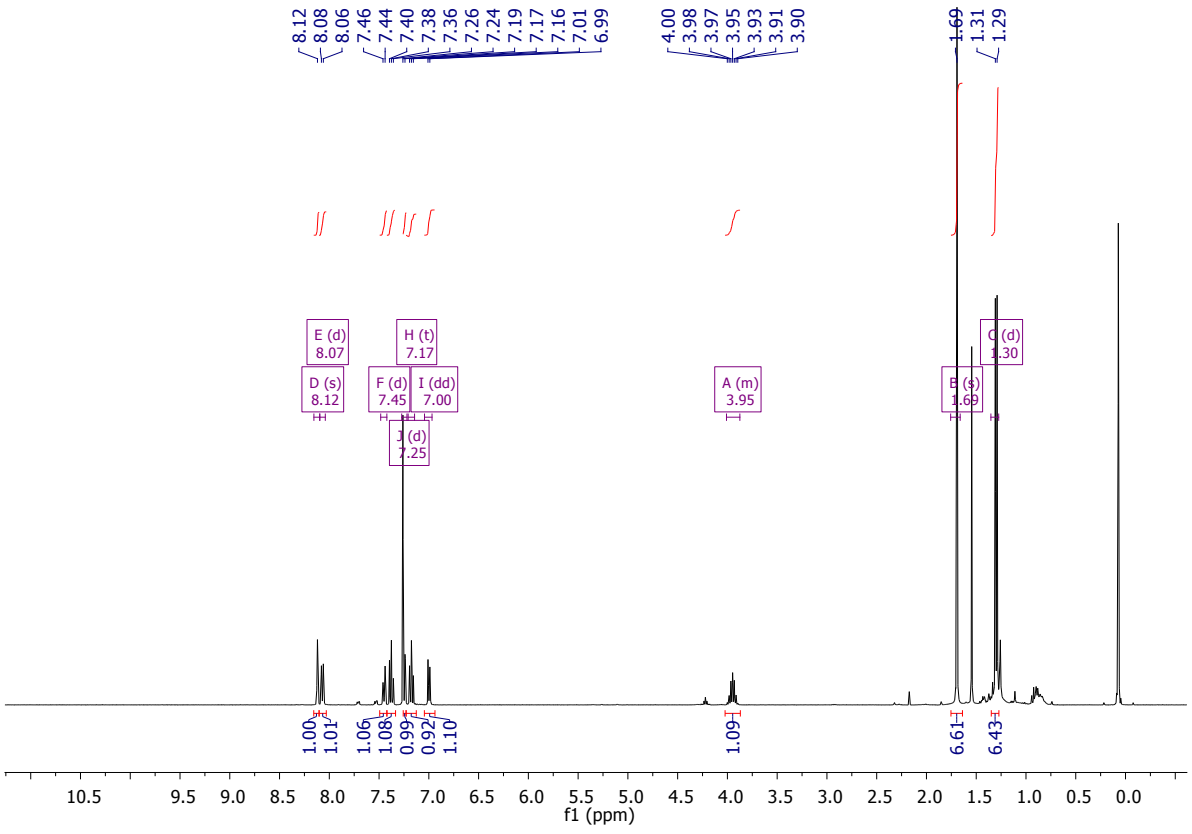

Figure S17. ^{1}H NMR spectrum of **5** (400 MHz, $CDCl_3$).

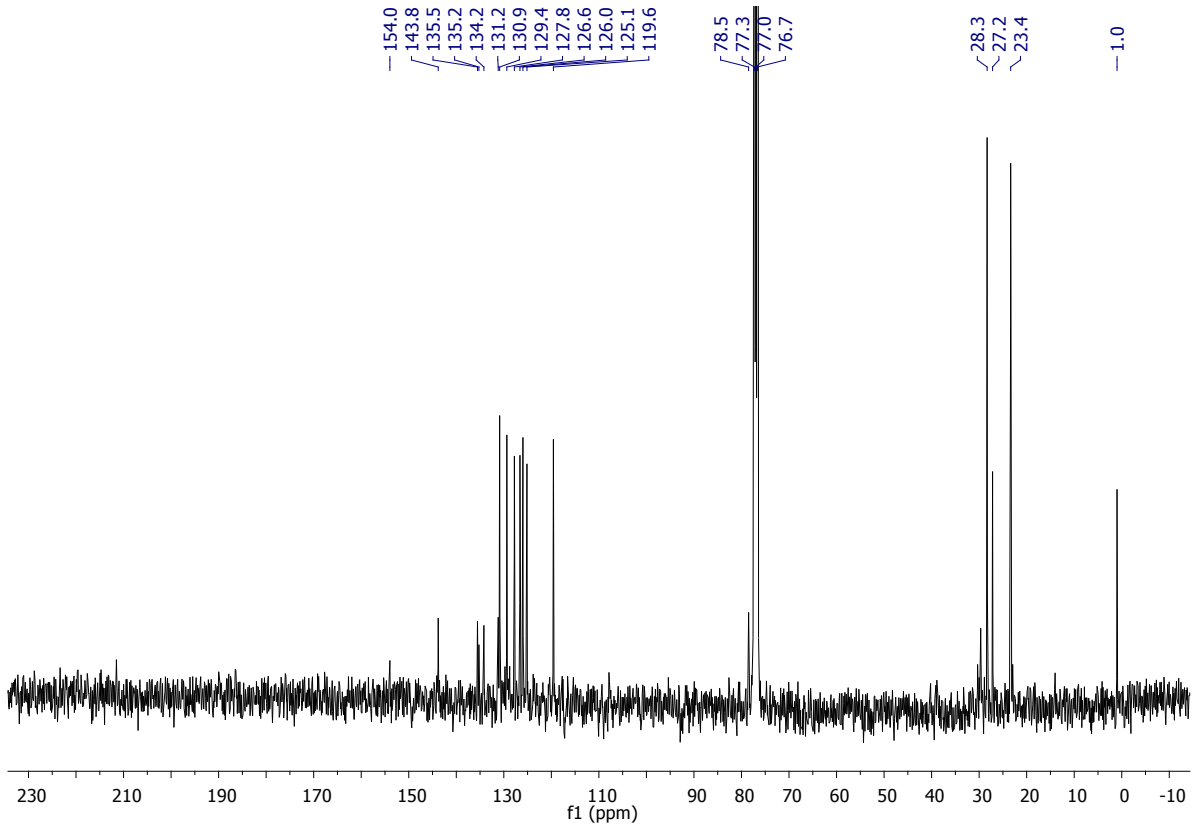

Figure S18. ^{13}C NMR spectrum of **5** (101 MHz, $CDCl_3$).

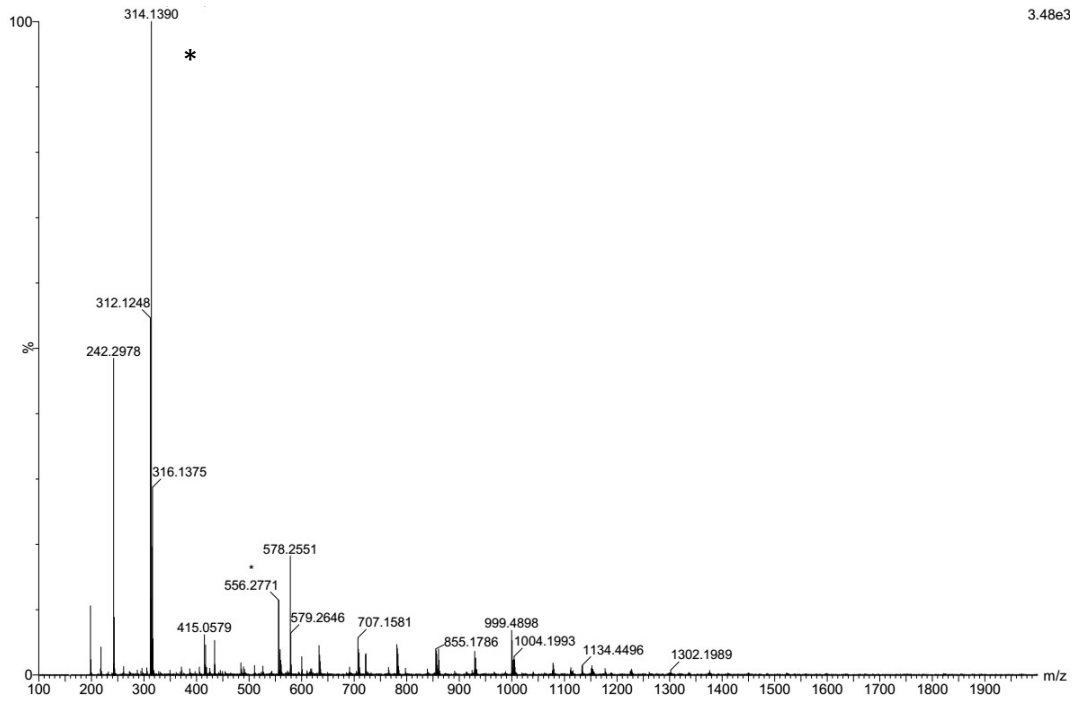

Figure S19. Positive mode ESI-MS spectrum of **5**; $[\mathbf{5} + H]^+$, $C_{19}H_{21}ClNO$ requires 314.1306.

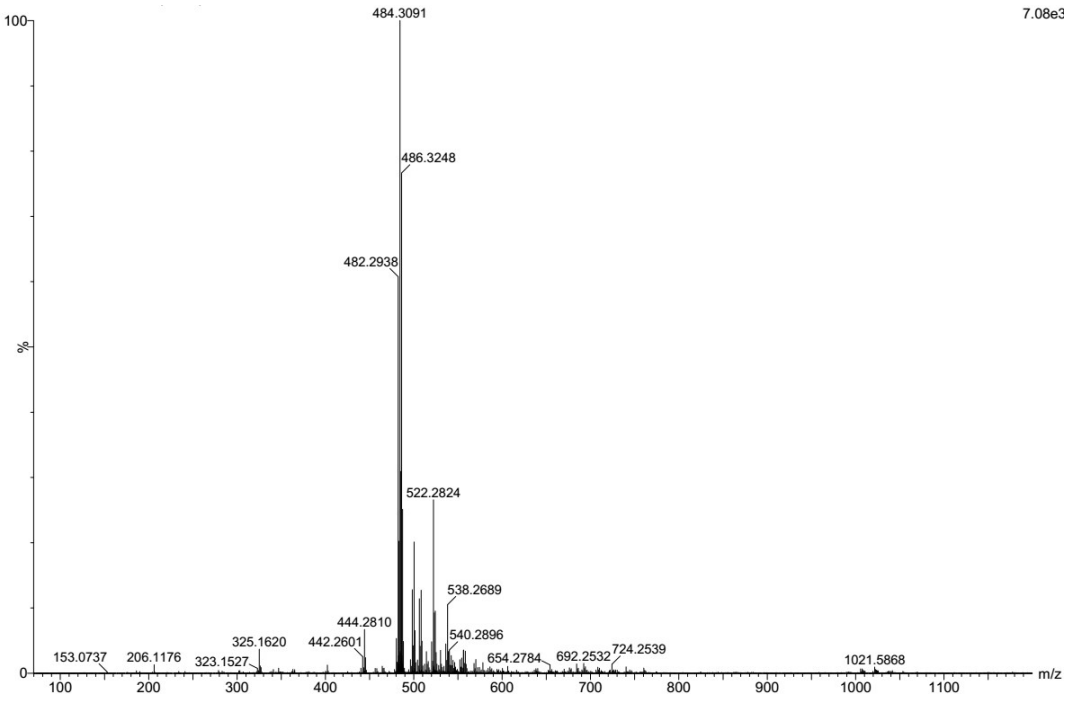

Figure S20. Positive mode ESI-MS spectrum of the post-decay (**1** + *m*-CPBA) mixture. The peak at 484.3091 corresponds to **4** ([**4** + H]$^+$, $C_{31}H_{38}N_3O_2$ requires 484.2964); the peak at 486.3248 corresponds to LH_2 (LH_3^+, $C_{31}H_{39}N_3O_2$, requires 486.3121.

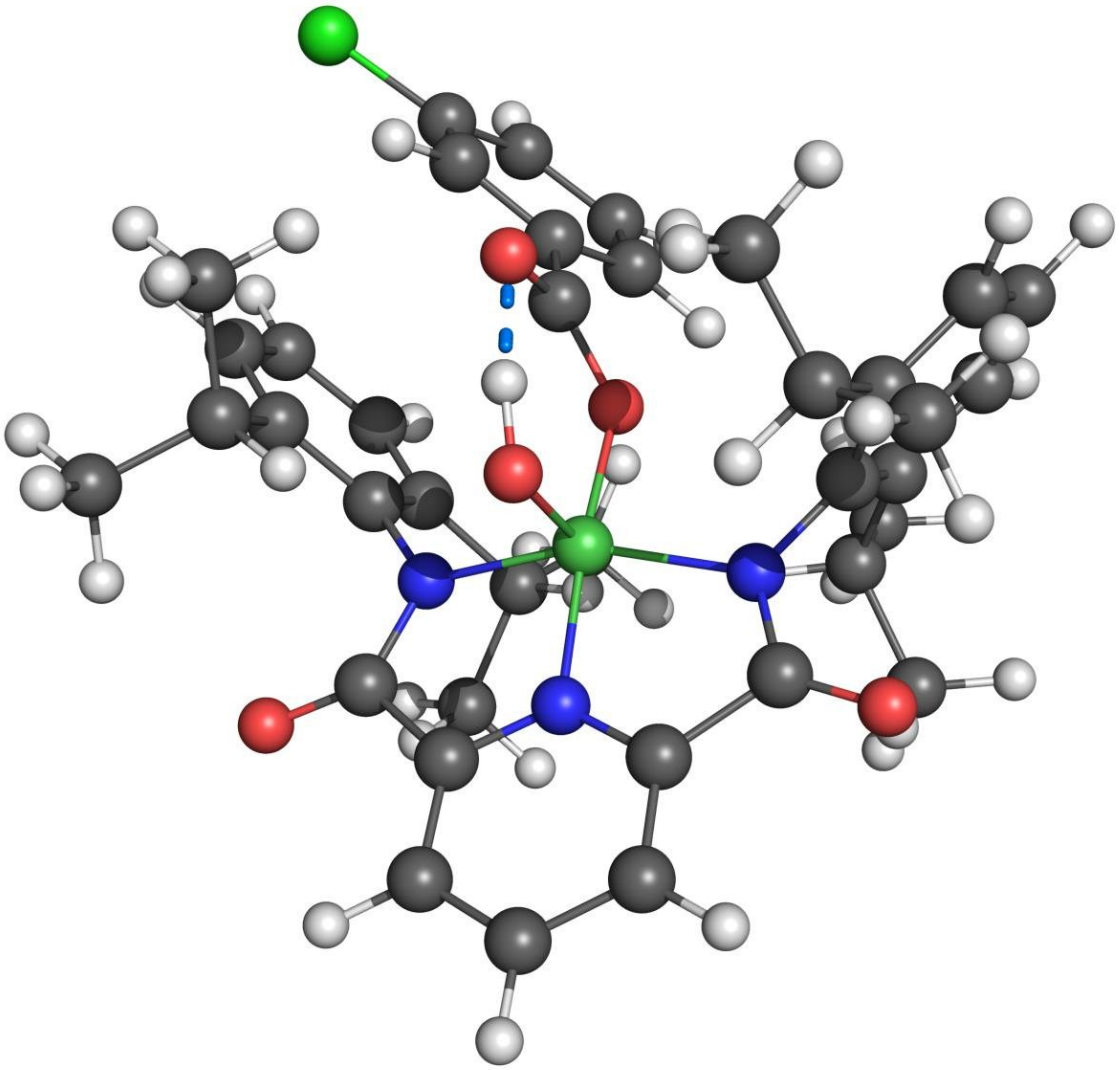

Figure S21. DFT-optimised structure obtained after binding of *m*-CPBA to **1**, in which the HO–OCOAr is broken spontaneously. The proton of the hydroxyl is involved in an intramolecular H-bond towards the *m*-CBA, which after proton transfer leads to the *m*-CBA and the Ni^{III}-oxyl species (obtained at BP86-D_3/TDZP, including COSMO solvation and ZORA relativistic effects self-consistently).

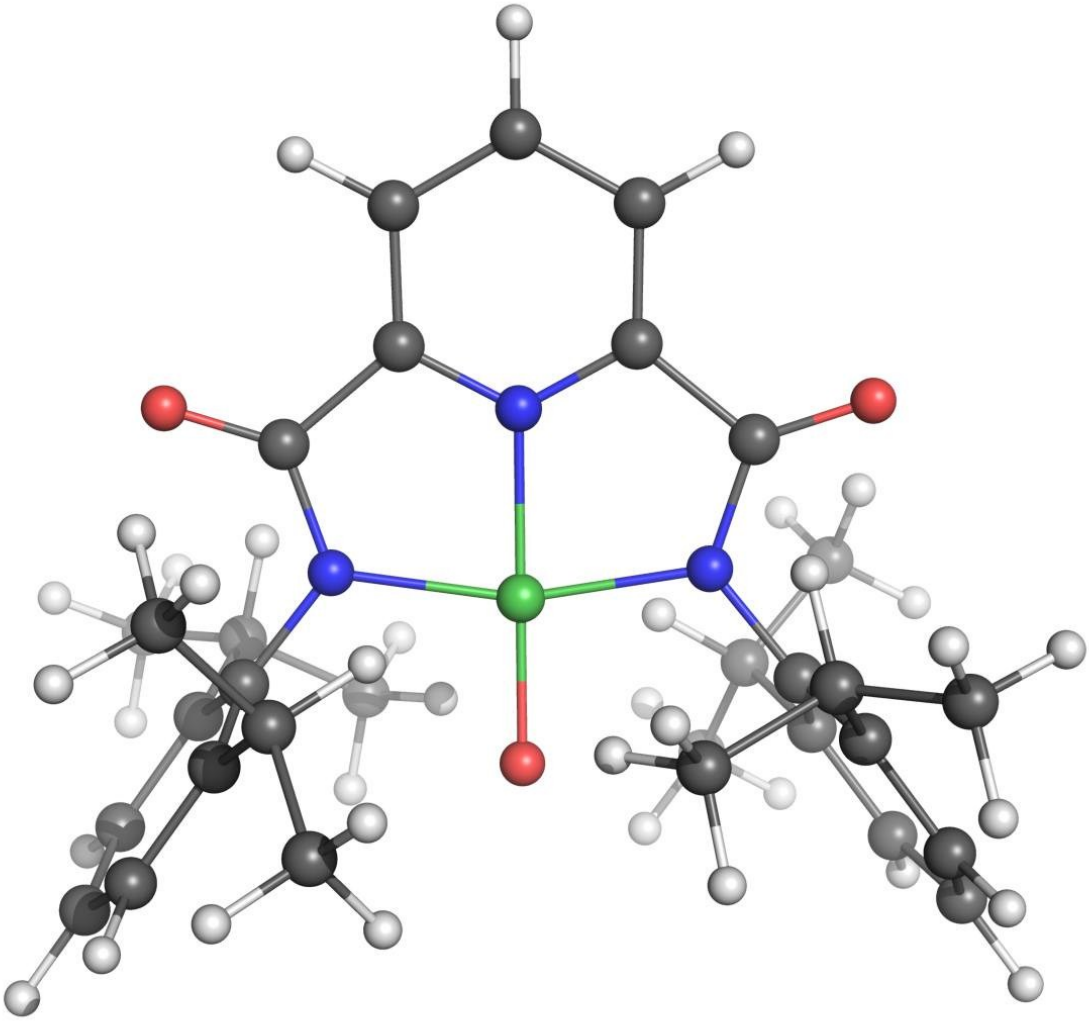

Figure S22. DFT-optimised Structure of the Ni^{III}-oxyl species (obtained at BP86-D_3/TDZP, including COSMO solvation and ZORA relativistic effects self-consistently).

All DFT calculations were performed with the Amsterdam Density Functional (ADF)[6] and QUILD[7] programs using the unrestricted Kohn-Sham scheme. Molecular orbitals were expanded in an uncontracted set of Slater type orbitals (STOs) of triple-ζ quality with double polarization functions (TZ2P), or the TDZP basis set which consists of triple-ζ quality on the metal and double-ζ quality on all other atoms, in both cases including one polarization function.[8] Core electrons were not treated explicitly during the geometry optimizations (frozen core approximation[6b]). An auxiliary set of s, p, d, f, and g STOs was used to fit the molecular density and to represent the Coulomb and exchange potentials accurately for each SCF cycle.

Geometries of all possible spin states were optimized with the QUILD[6] program using adapted delocalized coordinates until the maximum gradient component was less than 10^{-4} a.u.. Energies, gradients and Hessians[9] (for vibrational frequencies, including the Raman intensities) were calculated using BP86-D_3,[10] in all cases by including solvation effects through the COSMO[11] dielectric continuum model with appropriate parameters for the solvents.[12] For computing Gibbs free energies, all small frequencies were raised to 100 cm^{-1} in order to compensate for the breakdown of the harmonic oscillator model.[13] Scalar relativistic corrections have been included self-consistently in all calculations by using the zeroth-order regular approximation (ZORA).[14] The geometry optimizations at the BP86-D_3 level were performed with the TDZP basis set. Subsequent single-point calculations (with the TZ2P basis set) have been performed with S12g,[15] and all Time-Dependent DFT calculations were carried out with the SAOP potential[16] and the all-electron TZ2P basis set. For all calculations carried out with BP86-D_3 the Becke[17] grid of Normal quality was used; calculations performed with SAOP with a Becke grid of Good quality, and S12g calculations were performed with a Becke grid of VeryGood quality.

References

1. J. Wasilke, G. Wu, X. Bu, G. Kehr and G. Erker, *Organometallics*, 2005, **24**, 4289-4297.
2. S. Stoll and A. Schweiger, *J. Magn. Reson.*, 2006, **178**, 42-55.
3. C. Pramanik, S. Kotharkar, P. Patil, D. Gotrane, Y. More, A. Borhade, B. Chaugule, T. Khaladkar, K. Neelakandan, A. Chaudhari, M. G. Kulkarni, N. K. Tripathy and M. K. Gurjar, *Org. Process Res. Dev.*, 2014, **18**, 152-156.
4. Bruker APEX v2014.11-0, Bruker AXS Inc., Madison, Wisconsin, USA.
5. (a) SHELXL-2014, Bruker AXS Inc., Madison, Wisconsin, USA; (b) G. Sheldrick, *Acta Crystallogr. Sect. A*, 2008, **64**, 112-122.
6. (a) E. J. Baerends, T. Ziegler, J. Autschbach, D. Bashford, A. Berger, A. Bérces, F. M. Bickelhaupt, C. Bo, P. L. de Boeij, P. M. Boerrigter, S. Borini, R. E. Bulo, L. Cavallo, D. P. Chong, L. Deng, R. M. Dickson, A. C. T. van Duin, D. E. Ellis, M. v. Faassen, L. Fan, T. H. Fischer, C. Fonseca Guerra, A. Ghysels, A. Giammona, S. J. A. van Gisbergen, A. W. Götz, J. A. Groeneveld, O. V. Gritsenko, M. Grüning, S. Gusarov, F. E. Harris, T. Heine, P. van den Hoek, C. R. Jacob, H. Jacobsen, L. Jensen, E. S. Kadantsev, J. W. Kaminski, G. van Kessel, R. Klooster, F. Kootstra, A. Kovalenko, M. V. Krykunov, E. van Lenthe, J. N. Louwen, D. A. McCormack, E. McGarrity, A. Michalak, M. Mitoraj, J. Neugebauer, V. P. Nicu, L. Noodleman, V. P. Osinga, S. Patchkovskii, P. H. T. Philipsen, D. Post, C. C. Pye, W. Ravenek, J. I. Rodríguez, P. Romaniello, P. Ros, P. R. T. Schipper, G. Schreckenbach, J. S. Seldenthuis, M. Seth, D. G. Skachkov, J. G. Snijders, M. Solà, M. Swart, D. Swerhone, G. te Velde, P. Vernooijs, L. Versluis, L. Visscher, O. Visser, F. Wang, T. A. Wesolowski, E. M. van Wezenbeek, G. Wiesenekker, S. K. Wolff, T. K. Woo and A. L. Yakovlev, in *ADF2012.01*, SCM, Amsterdam, Editon edn., 2012; (b) G. te Velde, F. M. Bickelhaupt, E. J. Baerends, C. Fonseca Guerra, S. J. A. van Gisbergen, J. G. Snijders and T. Ziegler, *J. Comput. Chem.*, 2001, **22**, 931-967.
7. M. Swart and F. M. Bickelhaupt, *J. Comput. Chem.*, 2008, **29**, 724-734.
8. (a) E. van Lenthe and E. J. Baerends, *J. Comput. Chem.*, 2003, **24**, 1142-1156; (b) D. P. Chong, E. van Lenthe, S. J. A. van Gisbergen and E. J. Baerends, *J. Comput. Chem.*, 2004, **25**, 1030-1036.
9. S. K. Wolff, *Int. J. Quantum Chem.*, 2005, **104**, 645-659.
10. (a) A. D. Becke, *Phys. Rev. A*, 1988, **38**, 3098-3100; (b) J. P. Perdew, *Phys. Rev. B*, 1986, **33**, 8822-8824. Erratum: *Ibid*. 8834, 7406; (c) S. Grimme, J. Antony, S. Ehrlich and H. Krieg, *J. Chem. Phys.*, 2010, **132**, 154104.
11. A. Klamt and G. Schüürmann, *J. Chem. Soc. Perkin Trans. 2*, 1993, 799-805.
12. M. Swart, E. Rösler and F. M. Bickelhaupt, *Eur. J. Inorg. Chem.*, 2007, 3646-3654.
13. (a) B. B. Averkiev and D. G. Truhlar, *Catal. Sci. Technol.*, 2011, **1**, 1526-1529; (b) J. E. M. N. Klein, B. Dereli, L. Que Jr. and C. J. Cramer, *Chem. Commun.*, 2016, **52**, 10509-10512.
14. E. van Lenthe, E. J. Baerends and J. G. Snijders, *J. Chem. Phys.*, 1993, **99**, 4597-4610.
15. M. Swart, *Chem. Phys. Lett.*, 2013, **580**, 166-171.
16. P. R. T. Schipper, O. V. Gritsenko, S. J. A. van Gisbergen and E. J. Baerends, *J. Chem. Phys.*, 2000, **112**, 1344-1352.
17. (a) M. Franchini, P. H. T. Philipsen and L. Visscher, *J. Comput. Chem.*, 2013, **34**, 1819-1827; (b) A. Becke, *J. Chem. Phys.*, 1988, **88**, 2547-2553.